Hindawi
Geofluids
Volume 2022, Article ID 1481386, 10 pages
https://doi.org/10.1155/2022/1481386

Research Article

Active Earth Pressure for Sloping Finite Soil While Accounting for Shear Stress and Curved Slip Surface

Weiwei Wang,[1] Xinxi Liu,[1] Weidong Hu,[2] Hua Luo ,[2] and Guanghui Wang[2]

[1]*School of Civil Engineering, Changsha University of Science and Technology, Changsha 410114, China*
[2]*College of Civil Engineering and Architecture, Hunan Institute of Science and Technology, Yueyang 414000, China*

Correspondence should be addressed to Hua Luo; 12015024@hnist.edu.cn

Received 14 June 2022; Revised 30 July 2022; Accepted 29 August 2022; Published 15 September 2022

Academic Editor: Yi Xue

Calculating the earth pressure of the sloping soil having finite width behind the retaining wall is difficult for stability calculation. Thus, a novel method to calculate the active pressure of cohesionless sloping finite soil behind a retaining wall was developed to investigate. Taking cohesionless soil as the research object and considering the principal stress rotation of soil, the resultant force for active earth pressure, action point position, and earth pressure distribution of sloping finite soil was obtained based on assumptions of the translational mode of the rigid retaining wall and cycloidal slip surface. The accuracy of the proposed method was verified by model tests. The influence of the slope height ratio l/H and slope angle α on earth pressure was analyzed in this study. The result revealed that the horizontal component of the active earth pressure distribution curve for sloping finite soil was linear in area I and nonlinear with a drum shape in area II. There was a noticeable change at the junction of the two areas. The resultant force of earth pressure and the height of action point of resultant force increased and tended to reach a certain value as the aspect ratio l/H increased. When $l/H \geq 0.4$, the height of the action point of resultant force tended to be two-fifths the height of the wall. The resultant force and the height of the action point decreased linearly as the slope bottom angle increased.

1. Introduction

With the continuing development of capital construction projects in recent years, a significant number of retaining structures of high embankment retaining walls and adjacent foundation pits have appeared in the city [1]. Due to the influence of height difference and slope construction, the sloping finite soil forms behind the retaining wall. When the soil mass is destroyed, the sliding fracture surface ends at the slope surface, which contradicts the classical earth pressure theory [2, 3]. The distribution of horizontal earth pressure is assumed to be triangular in the classical earth pressure theory. However, the existing experimental findings [4–11] suggest that the horizontal earth pressure distribution is nonlinear. Moreover, scholars [6, 12–15] also considered the soil arch effect in calculating earth pressure.

The active earth pressure of finite soil between the rock face and the rigid retaining wall was studied by centrifugation tests [16, 17] and laboratory model tests [8, 18, 19]. The results revealed that finite soil has lower earth pressure than semi-infinite soil, and the distribution was nonlinear. Some scholars [20–25] have calculated the active earth pressure of finite soil by different methods. These researchers typically used the horizontal flat-element approach, and shear stress between soil layers was ignored in the force calculations. However, the horizontal shear stress between the element layers would be created by the primary stress deflection of the soil element induced by friction on the rear of the retaining wall ([26, 27]). In most research, finite soil's sliding surface was considered a plane. At the same time, some model experiments have demonstrated that the sliding surface is a curved surface [8, 11]. Based on the curved sliding surface, several researchers [8, 28, 29] developed a theoretical formula for the earth pressure of finite soil between a rock face and a solid retaining wall. However, these researches focused on finite width soil near the building or bedrock. In addition, research on active earth pressure of sloping finite soil behind the wall is uncommon.

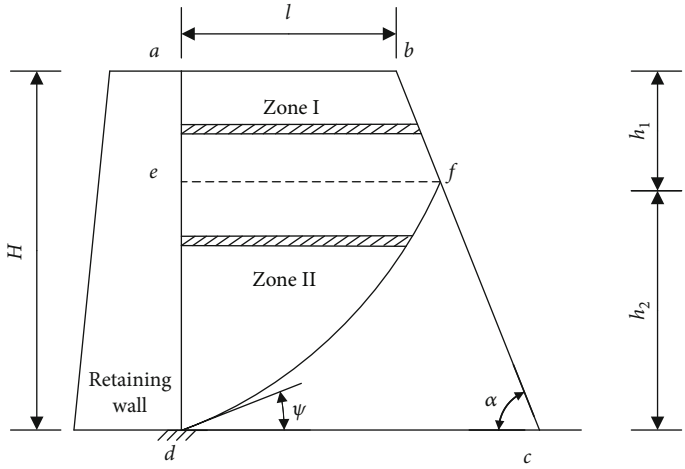

Figure 1: Calculation model of active earth pressure.

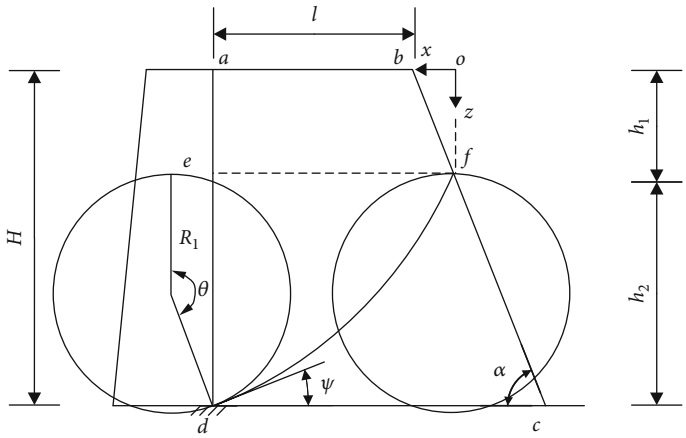

Figure 2: Slip surface through the slope surface.

Using the differential layer approach, scholars have conducted extensive studies on earth pressure distribution on finite soil. But the research on active earth pressure for sloping finite soil while accounting for shear stress and curved slip surface needs further development. Following methodology of Huang et al. [28], it was assumed in this study that the backfill had a cycloidal slip surface of the finite soil in translation mode. The horizontal flat-element method calculates the distribution of active earth pressure while accounting for the shear stress between the horizontal element layers; thus, an active earth pressure calculation model for sloping finite soil is established.

2. Calculation of Active Earth Pressure

A mechanical analysis model of finite soil is established, as shown in Figure 1. The retaining wall was positioned on the left side, and the cohesionless sloping finite soil was on the right side. The slope dip angle of finite soil is α, the slope top width is l, the gravity of soil is γ, the internal friction angle is φ, the depth of the retaining wall is H, and the external friction angle is δ. The sloping finite soil is divided into two zones, with the ef regarded as a dividing line. The height of zone I and zone II are h_1 and h_2, respectively, while the angle between the tangent line of any point on the slip surface and the horizontal direction is ψ.

There are four types of commonly applied curved slip surfaces of soil, including broken line sliding surface [20, 22, 24], logarithmic spiral curve [29], experimental fitting curve [8], and cycloidal curve [19, 30], as illustrated in Figure 2.

The equations of a cycloid line are as follows:

$$\begin{cases} x = R_1(\theta - \sin\theta), \\ z = R_1(1 - \cos\theta) + h_1, \end{cases} \tag{1}$$

where R_1 is the radius of the cycloid line and θ is the angle of the cycloid line.

When $z = H$, the initial angle of the cycloid line is θ_c, and the length of ef can be calculated as

$$\overline{\text{ef}} = R_1(\theta_c - \sin\theta_c). \tag{2}$$

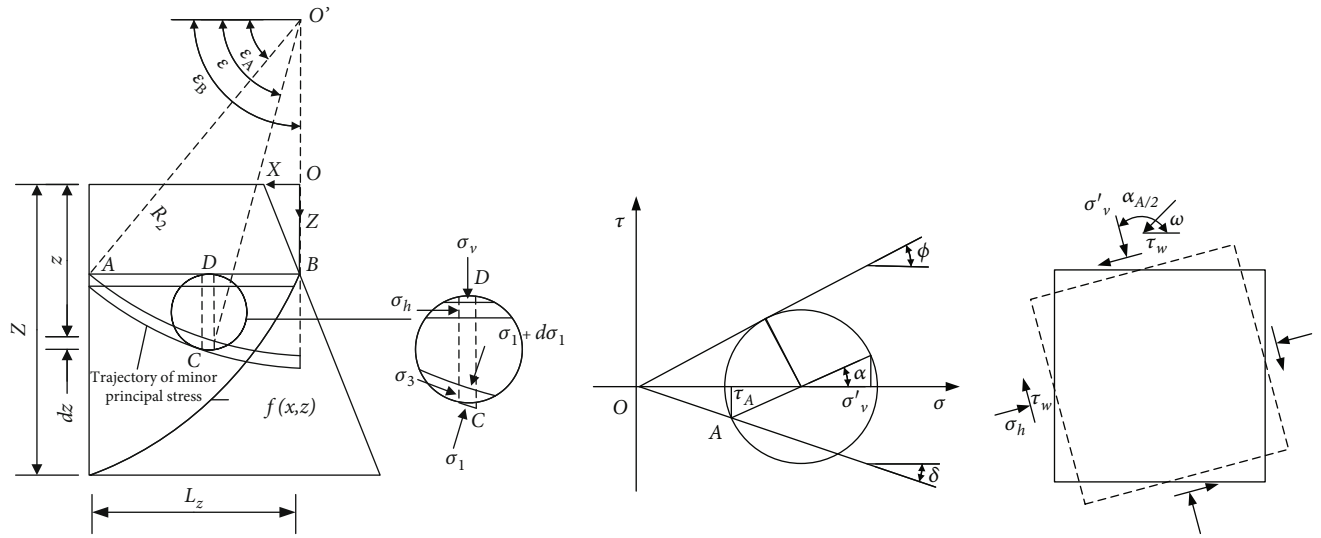

(a) Trajectory of minor principal stress

(b) Mohr's stress circle of soil at point A

Figure 3: Stress analysis of soil element.

It can also be obtained from the geometric relationship in Figure 2.

$$\left.\begin{aligned} \overline{\mathrm{cd}} &= l + \frac{H}{\tan\alpha}, \\ \overline{\mathrm{ed}} &= R_1(1-\cos\theta_c), \\ \overline{\mathrm{ef}} &= \overline{\mathrm{cd}} - \frac{\overline{\mathrm{ed}}}{\tan\alpha}. \end{aligned}\right\} \tag{3}$$

The radius of the cycloid line may be calculated using Equations (2) and (3).

$$R_1 = \frac{l + H/\tan\alpha}{\theta_c - \sin\theta_c + (1-\cos\theta_c)/\tan\alpha}. \tag{4}$$

The height of the cycloid slip surface is obtained as follows:

$$h_2 = \overline{\mathrm{ed}} = R_1(1-\cos\theta_c), \tag{5}$$

$$h_1 = H - h_2. \tag{6}$$

The slip surface of soil reaches the top of soil in the finite soil range when $h_2 \geq H$, which belongs to semi-infinite soil, where $h_1 = 0$. According to Equation (1), R_1 can be calculated as

$$R_1 = \frac{H}{1-\cos\theta_c}. \tag{7}$$

The rotation angle of the cycloid slip surface at any point is expressed as

$$\theta = \arccos\left(1 - \frac{z-h_1}{R_1}\right). \tag{8}$$

The slope of any point on the cycloid line is expressed as

$$\tan\psi = \frac{\mathrm{dz}}{\mathrm{dx}} = \tan\left(\frac{\pi}{2} - \frac{\theta}{2}\right). \tag{9}$$

At each point on the cycloid line, the angle between the tangent line and the horizontal direction equals

$$\psi = \frac{\pi}{2} - \frac{\theta}{2}. \tag{10}$$

Figure 3 depicts the horizontal differential layer AB, which is used as the study object and has a length of Lz and a height of dz at a distance of z from the soil surface. AB experiences stress deflection and produces an arc-shaped minor principal stress trajectory when the soil behind the retaining wall reaches the active limiting equilibrium state. The circle's center is at point O, and the radius is R_2. The angle between the horizontal direction and the connecting line from any point D in the arc to the center of the circle is ε, the angle between AO and the horizontal direction is ε_A, and the angle between BO and the horizontal direction is ε_B.

When the point D is in failure condition, its horizontal stress σ_h, vertical stress σ_v, and shear stress τ can be expressed as

$$\begin{cases} \dfrac{\sigma_v}{\sigma_1} = \sin^2\omega + K_a \cos^2\omega, \\ \dfrac{\sigma_h}{\sigma_1} = \cos^2\omega + K_a \sin^2\omega, \\ \dfrac{\tau}{\sigma_1} = \dfrac{\sin\varphi \cdot \sin 2\omega}{1 + \sin\varphi}, \end{cases} \tag{11}$$

where σ_1 is the major principal stress in a differential element, ω is angle between the direction of major principal stress and horizontal direction at point D, and K_a is the coefficient of passive earth pressure. Then,

$$K_a = \frac{\sigma_3}{\sigma_1} = \frac{1 - \sin\varphi}{1 + \sin\varphi}, \tag{12}$$

where σ_3 is the minor principal stress in a differential element.

Vertical resultant force dV at point D can be expressed as

$$\mathrm{dV} = \sigma_V \mathrm{dA} = \frac{\sigma_1[1 - \cos(2\omega)\sin\varphi]}{1 + \sin\varphi} R_2 \sin\omega d\omega, \tag{13}$$

where ε_A is the angle between the minor principal stress at A point and the horizontal plane and ε_B is the angle between the minor principal stress at B point and the horizontal plane.

When AB is in zone I, Equation (14) can be obtained:

$$\begin{aligned} \varepsilon_A &= \frac{\pi}{2} - \frac{\alpha_\mathrm{A}}{2}, \\ \varepsilon_B &= \frac{\pi}{2}, \end{aligned} \tag{14}$$

where $\alpha_\mathrm{A} = \arcsin(\sin\delta/\sin\varphi) - \delta$.

When AB is in zone II, ε_A is consistent with zone I.

$$\varepsilon_B = \frac{\pi}{4} - \frac{\varphi}{2} + \psi. \tag{15}$$

The lateral active earth pressure coefficient is the ratio of σ_h to the average vertical pressure $\overline{\sigma_v}$, as follows:

$$K_\mathrm{awn} = \frac{\sigma_h}{\overline{\sigma_v}} = \frac{\cos^2\varepsilon_A + K_a \sin^2\varepsilon_A}{1 + (((\cos^3\varepsilon_A - \cos^3\varepsilon_B)(K_a - 1))/(3(\cos\varepsilon_A - \cos\varepsilon_B)))}. \tag{16}$$

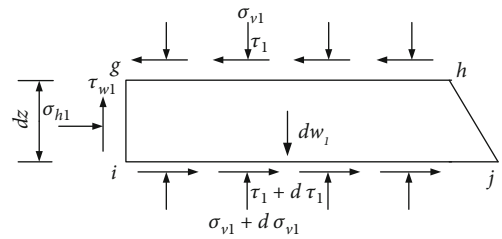

Figure 4: Stresses acting on horizontal elements in zone I.

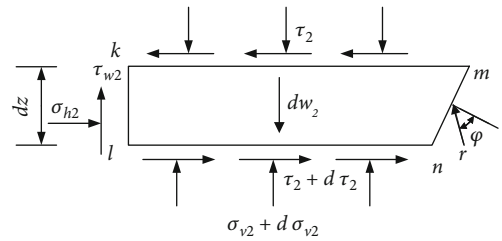

Figure 5: Stresses acting on horizontal elements in zone II.

The shear stress coefficient A can be calculated in the same way as follows:

$$\bar{\tau} = \frac{\int_{\varepsilon_A}^{\varepsilon_B} \tau R_2 \sin\varepsilon d\varepsilon}{L_z} = \frac{2\sin\varphi(\sin^3\varepsilon_A - \sin^3\varepsilon_B)}{3(1 + \sin\varphi)(\cos\varepsilon_A - \cos\varepsilon_B)}\sigma_1, \tag{17}$$

$$K_\tau = \frac{\bar{\tau}}{\overline{\sigma_v}} = \frac{2\sin\varphi(\sin^3\varepsilon_A - \sin^3\varepsilon_B)}{3(1 + \sin\varphi)(\cos\varepsilon_A - \cos\varepsilon_B) - 2\sin\varphi(\cos^3\varepsilon_A - \cos^3\varepsilon_B)}, \tag{18}$$

where $\bar{\tau}$ is the average shear stress on the principal stress trajectory.

As shown in Figure 4, a stress analysis is performed on the horizontal differential layer element in zone I.

The following formula can be obtained:

$$\sigma_{h1}\mathrm{dz} + \tau_1 \mathrm{dz}\cot\alpha + d\tau_1(l + z\cot\alpha) = 0, \tag{19}$$

where σ_{h1} is the horizontal active earth pressure at the depth z and τ_1 is the shear stress on the surface of the horizontal element. Assuming that τ_1 is uniformly distributed, it can be stated as follows:

$$\tau_1 = \sigma_{v1} K_\tau. \tag{20}$$

It can be concluded from the horizontal element's vertical static equilibrium condition that

$$\tau_{w1}\mathrm{dz} + \sigma_{v1}\mathrm{dz}\cot\alpha + d\sigma_{v1}(l + z\cot\alpha) - \mathrm{dw}_1 = 0. \tag{21}$$

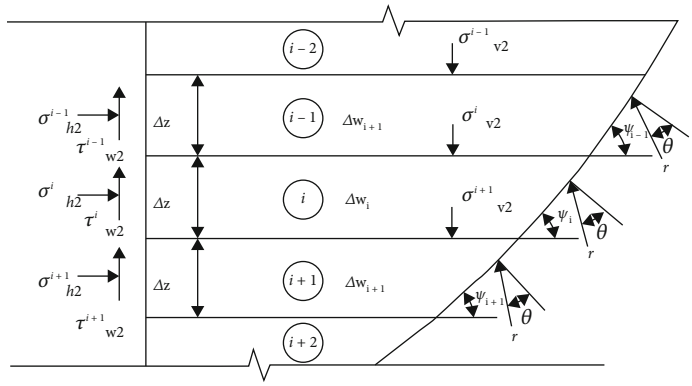

Figure 6: Stress of horizontal differential element layers.

where τ_{w1} is the friction shear stress on the interface between the retaining wall and the soil, which can be stated as

$$\tau_{w1} = \sigma_{h1} \tan \delta. \tag{22}$$

In addition, dw_1 is the self-weight of the horizontal differential element in zone I, and it is formulated as

$$dw_1 = \gamma(l + z \cot \alpha)dz. \tag{23}$$

Considering all the above conditions, the differential equation can be expressed as

$$\begin{cases} \dfrac{d\sigma_{v1}}{dz} = \gamma - \dfrac{\sigma_{h1} \tan \delta + \sigma_{v1} \cot \alpha}{l + z \cot \alpha}, \\ \sigma_{h1} = \dfrac{K_\tau \gamma (l + z \cot \alpha)}{K_\tau \tan \delta - 1}. \end{cases} \tag{24}$$

As shown in Figure 5, a stress analysis is performed on zone II's horizontal differential layer element. It can be obtained from the geometric relationship in Figure 5.

$$\left.\begin{aligned} \overline{kl} &= l + h_1 \cot \alpha - R_1(\theta - \sin \theta), \\ \overline{mn} &= \overline{kl} - \cot \psi dz = \overline{kl} - \tan \frac{\theta}{2} dz. \end{aligned}\right\} \tag{25}$$

By omitting the second derivative, the following equation is obtained:

$$\sigma_{h2}dz + \tau_2 \overline{kl} - (\tau_2 + d\tau_2)\overline{mn} - \frac{r \cos(\pi/2 + \varphi - \psi)dz}{\sin \psi} = 0, \tag{26}$$

where σ_{h2} is the horizontal active earth pressure, r is the reaction force on the sliding inclined plane, σ_{v2} is the average vertical normal stress on the surface of the horizontal element, and τ_2 is the horizontal shear stress on the surface of the horizontal element.

$$\tau_2 = \sigma_{v2} K_\tau. \tag{27}$$

Table 1: List of tests.

Test number	The height of soil (m)	The top width of slope (m)	The bottom angle of slope
1	0.500	0.050	33.7°
2	0.500	0.100	33.7°
3	0.500	0.150	33.7°

Based on the horizontal element's vertical static equilibrium condition, it can be determined that

$$dw_2 - \sigma_{v2}\overline{kl} + (\sigma_{v2} + d\sigma_{v2})\overline{mn} - \tau_{w2}dz - \frac{r \sin(\pi/2 + \varphi - \psi)dz}{\sin \psi} = 0, \tag{28}$$

where τ_{w2} is the friction shear stress on the interface between the retaining wall and the soil mass; it can be stated as follows:

$$\tau_{w2} = \sigma_{h2} \tan \delta, \tag{29}$$

where dw_2 is the self-weight of the horizontal layer unit in zone II, which can be stated as

$$dw_2 = \frac{\gamma}{2}\left(\overline{kl} + \overline{mn}\right)dz. \tag{30}$$

Formulas (25)–(30) are synthesized as follows:

$$\begin{aligned} \frac{d\sigma_{v2}}{dz}\overline{kl}\left[1 + K_\tau \tan\left(\varphi + \frac{\theta}{2}\right)\right] &= \gamma\overline{kl} + \sigma_{v2}\left[\tan\frac{\theta}{2} - K_{awn}\tan\delta - K_{awn}\tan\left(\varphi + \frac{\theta}{2}\right)\right. \\ &\quad \left. + K_\tau \tan\frac{\theta}{2}\tan\left(\varphi + \frac{\theta}{2}\right)\right], \end{aligned} \tag{31}$$

$$\frac{d\sigma_{v2}}{dz} = \frac{1}{A}\gamma + \frac{B}{A\overline{kl}}\sigma_{v2}, \tag{32}$$

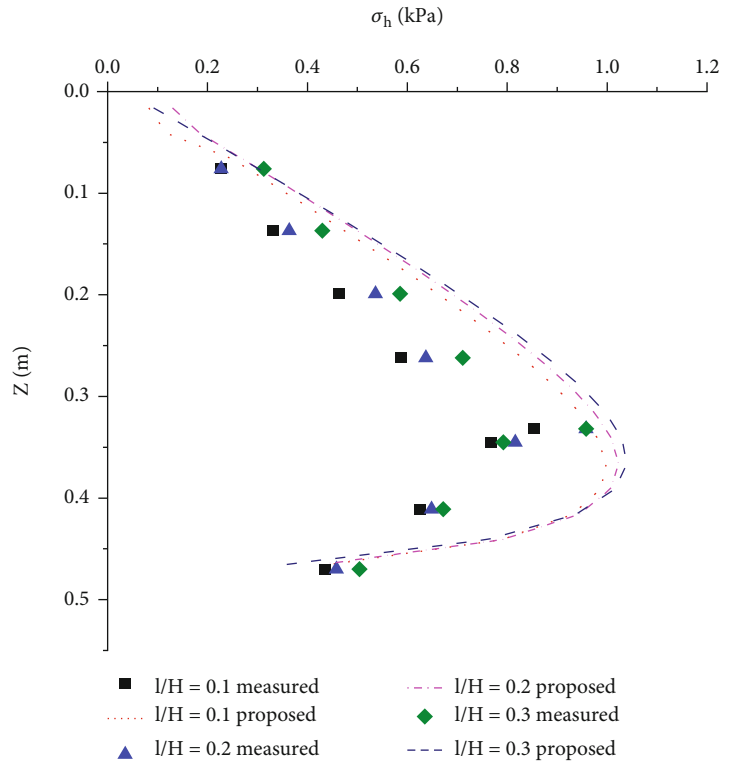

Figure 7: Comparison of the proposed model's results and the experimental validation of the laboratory test.

in which

$$\left.\begin{aligned} A &= 1 + K_\tau \tan\left(\varphi + \frac{\theta}{2}\right), \\ B &= \tan\frac{\theta}{2} - K_{\text{awn}} \tan\left(\varphi + \frac{\theta}{2}\right) - K_{\text{awn}} \tan\delta + K_\tau \tan\frac{\theta}{2} \tan\left(\varphi + \frac{\theta}{2}\right). \end{aligned}\right\} \tag{33}$$

The difference method is used to estimate a solution that can be achieved using the finite difference method. The soil mass is divided into several horizontal differential element layers. The thickness of each layer is Δz, as shown in Figure 6.

Equation (31) can be expressed as

$$\begin{cases} \dfrac{\Delta\sigma^i{}_{v2}}{\Delta z} = \dfrac{1}{A}\gamma + \dfrac{B}{A\bar{k}\bar{l}}\sigma^i{}_{v2}, \\ \sigma^{i+1}{}_v = \sigma^i{}_v + \Delta\sigma^i{}_v, \\ \sigma^{i+1}{}_{h2} = K_{\text{awn}}\sigma^{i+1}{}_{v2}, \end{cases} \tag{34}$$

where $\sigma^1{}_v$ is expected to be q in the condition of $Z = 0$, and the corresponding values of $\sigma^i{}_v$ for different soil strips can be calculated according to Equation (24) and Equation (34). Afterwards, the values of $\sigma^i{}_h$ and τ^i_w for all horizontal layers can be computed sequentially. On this basis, the resultant force and overturning moment of earth pressure are obtained according to the following:

$$\begin{cases} E = \sum_{i=1}^{n} \dfrac{\sigma^i{}_h}{\cos\delta}\Delta z, \\ M = \sum_{i=1}^{n} \sigma^i{}_h\left(H - z^i\right)\Delta z, \end{cases} \tag{35}$$

where n is the number of horizontal layers, z^i is the vertical distance between the center of the i^{th} layer and the top surface of the soil, and ψ is the angle between the direction of the resultant force and the horizontal direction. The vertical distance between the resultant force's action point and the wall heel is defined as

$$h = \frac{M}{E\cos\delta} = \frac{\sum_{i=1}^{n}\sigma^i{}_h\left(H - z^i\right)}{\sum_{i=1}^{n}\sigma^i{}_h}. \tag{36}$$

3. Experimental Comparison

The proposed approach's computation outcomes are compared to laboratory test results to ensure its applicability. Three groups of experiments were performed by using cohesionless sand. The geometric parameters of the tests are shown in Table 1. The internal friction angle is $\varphi = 39.6°$, the gravity is $\gamma = 16.1\,\text{kN/m}^3$, and the outer friction angle is $\delta = 2/3\varphi$.

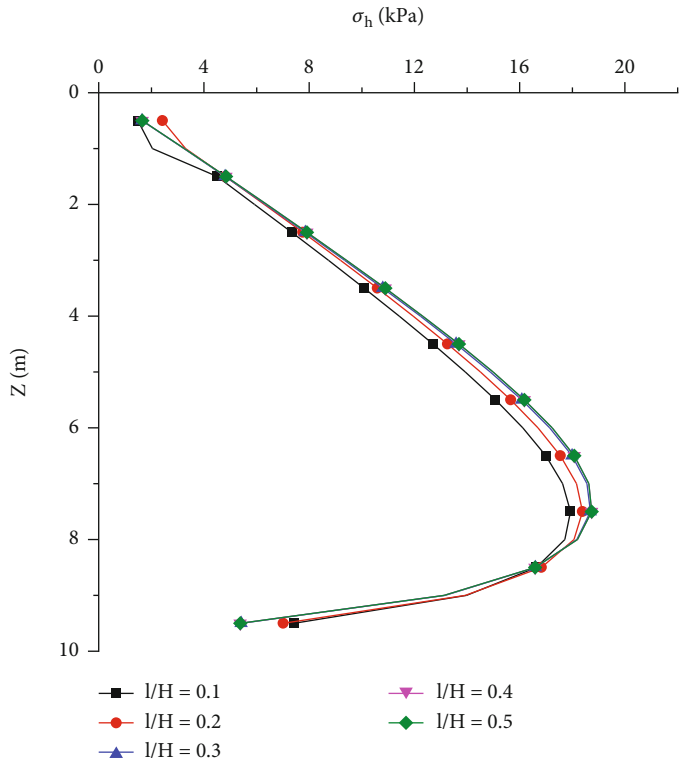

Figure 8: Distribution of active earth pressure under different l/H ($\alpha = 40$).

As illustrated in Figure 7, the theoretical calculation results of the distribution of active earth pressure were compared with the experimental results.

It can be demonstrated that the proposed approach produces a distribution of active earth pressure that was comparable to the findings of laboratory model experiments. The earth pressure distribution curve was found to be nonlinear and drum-shaped. The active earth pressure determined by the model test on sloping finite soil was relatively close to the proposed calculated value. However, some discrepancies may be attributable to the influence of test boundary conditions and parameters.

4. Parameter Analysis

In this section, the influences of geometric slope parameters on the distribution, resultant force, and action point of active earth pressure are evaluated. Assuming that the sloping finite soil behind the retaining wall is cohesionless, the wall's back is defined as vertical, and its height is defined as 10 m. The soil gravity is 17.0 kN/m^3, the internal friction angle is $\varphi = 43^\circ$, and the external friction angle is $\delta = 2/3\varphi$.

4.1. Analysis of the Distribution of Earth Pressure. Figure 8 illustrates the influence of different l/H on the distribution of active earth pressure with $\alpha = 40^\circ$. The distribution of active earth pressure in zone I is linear; however, it is nonlinear with a drum shape in zone II.

A sharp change at the junction of the two zones was observed. The horizontal component of active earth pressure

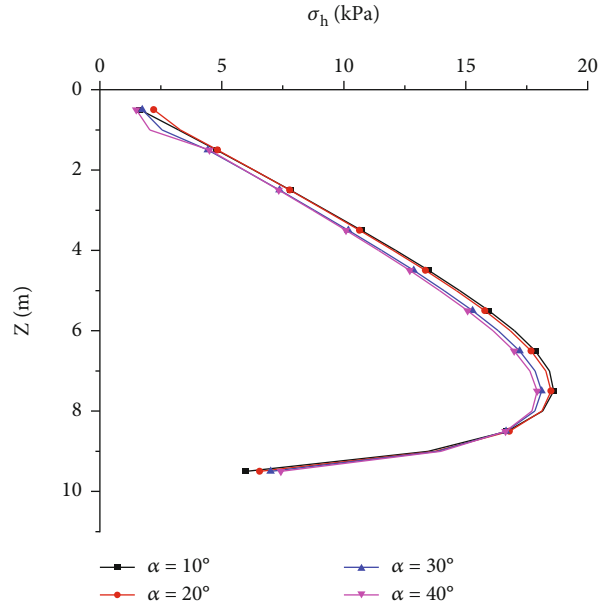

Figure 9: Distribution of active earth pressure under different α ($l/H = 0.1$).

increased gradually with an increase in the aspect ratio l/H. When $l/H > 0.4$, it tended to be stable and could be regarded as semi-infinite soil. Figure 9 demonstrates the influence of different α on the distribution of the horizontal component of active earth pressure with $l/H = 0.1$. The

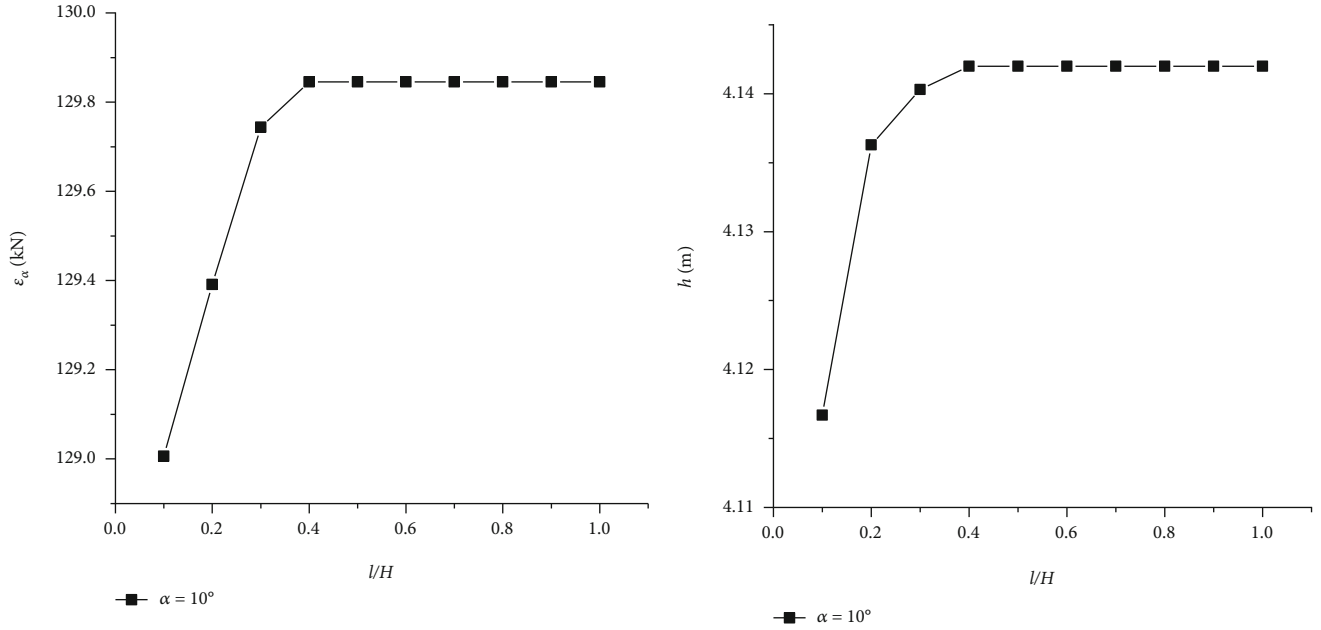

(a) Effect of l/H on the resultant force

(b) Effect of l/H on the position of resultant force

Figure 10: Effect of l/H on active earth pressure.

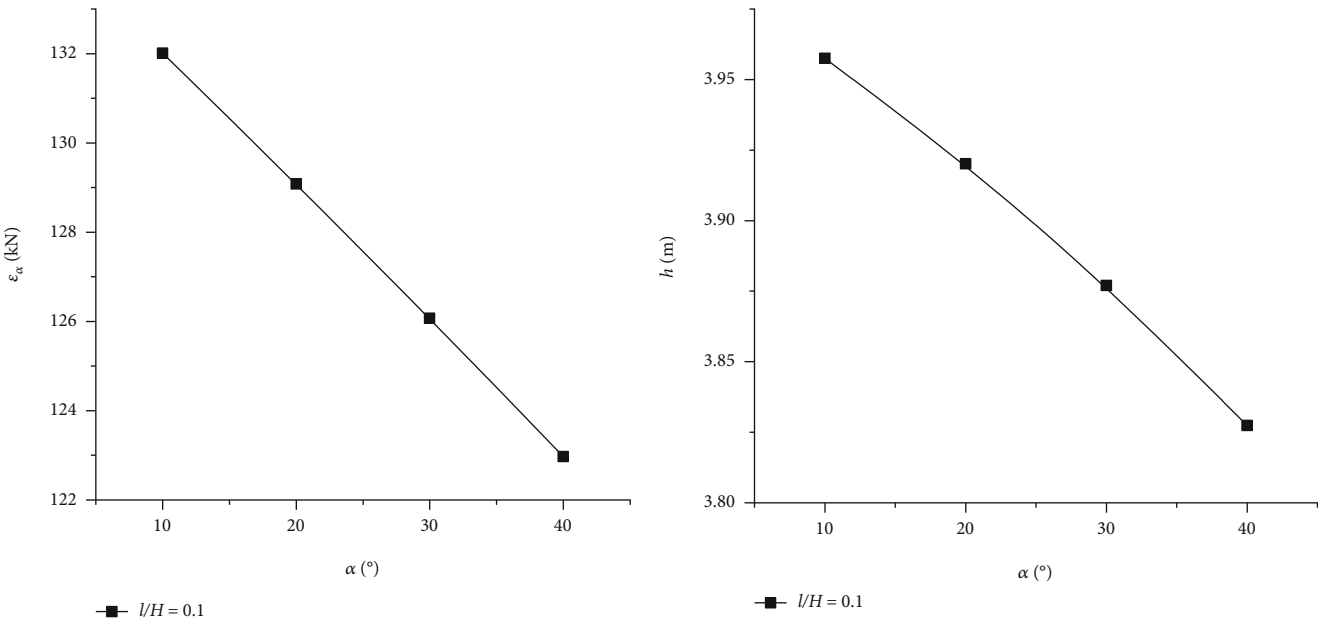

(a) Effect of α on the resultant force

(b) Effect of α on the position of resultant force

Figure 11: Effect of α on active earth pressure.

horizontal component of active earth pressure gradually declined as α increased, particularly in zone I.

4.2. Analysis of Resultant Force and Earth Pressure. Figure 10 depicts the impact of various l/H on the resultant earth pressure and its action point height. The resultant force of finite earth pressure had an action point slightly greater than that calculated by Coulomb's theory. In the case of $l/H < 0.4$, the resultant force and its action point of active earth pressure increased nonlinearly with an increase in the aspect ratio. On the other hand, for $l/H \geq 0.4$, the resultant force and its action point of active earth pressure tended to be stable, and slope finite soil could be regarded as semi-infinite soil.

Figure 11 shows the influence of different α on the resultant earth pressure and its action point height. The resultant force of active earth pressure declined linearly as α increased,

and the acting point height of the resultant force of earth pressure similarly decreased, which was approximately two-fifths the height of the wall.

5. Conclusions

In the current study, a calculation method was developed for the soil pressure of a sloping finite soil, considering the shear stress and the curved slip surface. To validate the rationality of these formulas, the earth pressure distribution was compared to current test outcomes.

With the increase in aspect ratio, the horizontal component of the active earth pressure distribution curve was linear in zone I and nonlinear with a drum shape in zone II. Besides, a noticeable change at the junction of the two zones was observed. The change became weaker as the aspect ratio l/H decreased and stronger as α increased.

The resultant force of earth pressure and the position of the resultant force action point increased and tended to achieve a specific value as the aspect ratio l/H increased. With an increase in α, the resultant force and the height of the resultant force acting point were reduced linearly.

Data Availability

Some or all data, models, or code that support the findings of this study are available from the corresponding author upon reasonable request.

Conflicts of Interest

The authors declare that they have no conflicts of interest.

Acknowledgments

The financial support from the National Natural Science Foundation of China (NSFC Grant 51676041), Natural Science Foundation of Hunan Province, China (Grant No. 2020JJ5216), and Scientific Research Foundation of Hunan Provincial Education Department, China (Grant Nos. 19A208 and 20A228) is gratefully acknowledged.

References

[1] C. Y. Liu, Y. Wang, X. M. Hu, Y. L. Han, X. P. Zhang, and L. Z. du, "Application of GA-BP neural network optimized by Grey Verhulst model around settlement prediction of foundation pit," *Geofluids*, vol. 2021, Article ID 5595277, 16 pages, 2021.

[2] C. A. Coulomb, "Essais sur une application des regles des maximis etminimis a quelques problems de statique relatits a l'architecture," *[In French.] Memoires de l'Academie Royale des Sciences presentespar divers Savans*, vol. 7, pp. 343–382, 1776.

[3] W. J. M. Rankine, "On the stability of loose earth. Philosophical transactions," *Royal Society of London*, vol. 147, no. 147, pp. 9–27, 1857.

[4] M. F. Chang, "Lateral earth pressures behind rotating walls," *Canadian Geotechnical Journal*, vol. 34, no. 4, pp. 498–509, 1997.

[5] Y. S. Fang and I. Ishibashi, "Static earth pressures with various wall movements," *Journal of Geotechnical Engineering*, vol. 112, no. 3, pp. 317–333, 1986.

[6] C. Liu, L. Du, X. Zhang, Y. Wang, X. Hu, and Y. Han, "A new rock brittleness evaluation method based on the complete stress-strain curve," *Lithosphere*, vol. 2021, no. Special 4, article 4029886, 2021.

[7] T. S. O'Neal and D. J. Hagerty, "Earth pressures in confined cohesionless backfill against tall rigid walls—a case history," *Canadian Geotechnical Journal*, vol. 48, no. 8, pp. 1188–1197, 2011.

[8] R. Rui, Y. Q. Ye, J. Han, L. Zhang, and Y. X. Zhai, "Experimental and theoretical investigations on active earth pressure distributions behind rigid retaining walls with narrow backfill under a translational mode," *International Journal of Geomechanics*, vol. 20, no. 10, article 04020178, 2020.

[9] M. A. Sherif and Y. S. Fang, "Dynamic earth pressures on walls rotating about the top," *Soils and Foundations*, vol. 24, no. 4, pp. 109–117, 1984.

[10] Z. V. Tsagareli, "Experimental investigation of the pressure of a loose medium on retaining walls with a vertical back face and horizontal backfill surface," *Soil Mechanics and Foundation Engineering*, vol. 2, no. 4, pp. 197–200, 1965.

[11] G. Yang, Y. Y. Wang, and Y. C. Liu, "Analysis of active earth pressure on retaining walls based on curved sliding surface," *[In Chinese.] Rock and Soil Mechanics.*, vol. 38, no. 8, pp. 2182–2188, 2017.

[12] S. Goel and N. R. Patra, "Effect of arching on active earth pressure for rigid retaining walls considering translation mode," *International Journal of Geomechanics*, vol. 8, no. 2, pp. 123–133, 2008.

[13] R. L. Handy, "The arch in soil arching," *Journal of Geotechnical Engineering*, vol. 111, no. 3, pp. 302–318, 1985.

[14] W. D. Hu, K. X. Liu, X. N. Zhu, X. L. Tong, and X. Zhou, "Active earth pressure against rigid retaining walls for finite soils in sloping condition considering shear stress and soil arching effect," *Advances in Civil Engineering*, vol. 2020, Article ID 6791301, 11 pages, 2020.

[15] Y. T. Zhou, Q. S. Chen, F. Q. Chen, X. H. Xue, and S. Basack, "Active earth pressure on translating rigid retaining structures considering soil arching effect," *European Journal of Environmental and Civil Engineering*, vol. 22, no. 8, pp. 910–926, 2018.

[16] S. Frydman and I. Keissar, "Earth pressure on retaining walls near rock faces," *Journal of Geotechnical Engineering*, vol. 113, no. 6, pp. 586–599, 1987.

[17] W. A. Take and A. J. Valsangkar, "Earth pressures on unyielding retaining walls of narrow backfill width," *Canadian Geotechnical Journal*, vol. 38, no. 6, pp. 1220–1230, 2001.

[18] W. D. Hu, X. N. Zhu, X. H. Liu, Y. Q. Zeng, and X. Y. Zhou, "Active earth pressure against cantilever retaining wall adjacent to existing basement exterior wall," *International Journal of Geomechanics*, vol. 20, no. 11, p. 04020207, 2020.

[19] M. Yang and X. Tang, "Rigid retaining walls with narrow cohesionless backfills under various wall movement modes," *International Journal of Geomechanics*, vol. 17, no. 11, pp. 04017098.1–04017098. 11, 2017.

[20] F. Chen, J. Yang, and Y. Lin, "Active earth pressure of narrow granular backfill against rigid retaining wall near rock face under translation mode," *International Journal of Geomechanics*, vol. 19, no. 12, pp. 04019133.1–04019133. 13, 2019.

[21] S. Ghobadi and H. Shahir, "Analytical solution for active pressure of narrow backfills considering arching effect," *Engineering Computations*, vol. 38, no. 1, pp. 221–241, 2020.

[22] V. Greco, "Active thrust on retaining walls of narrow backfill width," *Computers and Geotechnics*, vol. 50, no. may, pp. 66–78, 2013.

[23] Y.-Y. Jiao, Y. Zhang, and F. Tan, "Estimation of active earth pressure against rigid retaining walls considering soil arching effects and intermediate principal stress," *Journal of Geotechnical Engineering*, vol. 20, no. 11, p. 04020217, 2020.

[24] Y. J. Lin, F. Q. Chen, and J. T. Yang, "Inclined slice method to earth pressure of narrow cohesionless backfill against rigid walls under various displacement modes," *KSCE Journal of Civil Engineering*, vol. 24, no. 5, 2020.

[25] M. Xie, J. Zheng, R. Zhang, L. Cui, and C. Miao, "Active earth pressure on rigid retaining walls built near rock faces," *International Journal of Geomechanics*, vol. 20, no. 6, p. 04020061, 2020.

[26] W. Cao, H. Zhang, T. Liu, and X. Tan, "Analytical solution for the active earth pressure of cohesionless soil behind an inclined retaining wall based on the curved thin-layer element method," *Computers and Geotechnics*, vol. 128, no. 2020, article 103851, 2020.

[27] Z. Y. Liu, "Active earth pressure calculation of rigid retaining walls with limited granular backfill space," *[In Chinese.] China Journal of Highway and Transport*, vol. 31, no. 2, pp. 154–164, 2018.

[28] K. Huang, R. Liu, Y. Sun, L. Li, Y. Xie, and X. Peng, "Study on the calculation method of active earth pressure and critical width for finite soil behind the retaining wall," *Earth Science*, vol. 10, article 883668, 2022.

[29] M. H. Yang, X. C. Tang, and Z. Y. Wu, "Slip surface and active earth pressure of cohesionless narrow backfill behind rigid retaining walls under translation movement mode," *International Journal of Geomechanics*, vol. 20, no. 8, 2020.

[30] Z. M. Cao, "Active earth pressure analysis on retaining wall with sliding surface of filling curve," *[In Chinese.] China Journal of Highway and Transport*, vol. 8, no. 1, pp. 7–14, 1995.